

Cite this article as: Fu Xiujuan, Lu Jiang, Zhao Yan, et al. Influence of Initial Texture on Inhomogeneous Plastic Deformation of Tailor Rolled Blank[J]. Rare Metal Materials and Engineering, 2021, 50(08): 2721-2727.

ARTICLE

# Influence of Initial Texture on Inhomogeneous Plastic Deformation of Tailor Rolled Blank

Fu Xiujuan, Lu Jiang, Zhao Yan, Ye Gang

School of Materials Science and Engineering, Wuhan Institute of Technology, Wuhan 430073, China

**Abstract:** Different textures are formed in different thickness zones of CR340 tailor rolled blank (TRB) during rolling, including  $\{111\}\langle 0\bar{1}1\rangle$  and  $\{141\}\langle 2\bar{1}2\rangle$  textures in the thin zone,  $\{225\}\langle 1\bar{1}0\rangle$  and  $\{211\}\langle 0\bar{1}1\rangle$  textures in the transition zone, and  $\{876\}\langle 2\bar{2}5\rangle$  and  $\{411\}\langle 0\bar{1}1\rangle$  textures in the thick zone. The polycrystalline plastic finite element model in different thickness zones was established based on the results of EBSD test to study the influence of grain structure in different thickness zones on the activation of slip system and stress-strain distribution under uniaxial tension. The results show that the  $\{111\}\langle 0\bar{1}1\rangle$  texture of thin zone and  $\{876\}\langle 2\bar{2}5\rangle$  texture of thick zone are conducive to slip system activation, and 8 and 9 sets of slip systems are activated, respectively, which weaken stress concentration of equal thickness zone in the deformation process, so equal thickness zone has good plastic deformation behavior. However, the grain slip system of  $\{225\}\langle 1\bar{1}0\rangle$  and  $\{211\}\langle 0\bar{1}1\rangle$  textures in transition zone is less activated, and the number of activation is just 6 and 7, respectively, which lead to the high stress concentration, and thus the plastic deformation behavior is poor. The TRB presents obvious non-uniformity in plastic deformation because of the difference in texture of each thickness region, and the fracture position of the TRB appears in the transition zone with poor plastic deformation during uniaxial tension.

**Key words:** tailor rolled blank (TRB); crystal plasticity finite element method; texture; plastic deformation; slip system

Tailor rolled blank (TRB) is one of the most potential lightweight blanks<sup>[1,2]</sup>, whose thickness is continuously changed by real-time adjustment of the roll gap in the rolling process. The different thickness zones are subjected to different degrees of rolling, so preferred crystallographic orientation of each thickness zone is different<sup>[3,4]</sup>. Due to the difference in microstructure and mechanical properties of the different thickness zones, the inhomogeneous plastic deformation behavior of TRB occurs in forming, which makes TRB prone to form defects such as wrinkling, cracking and spring-back<sup>[5-7]</sup>. Therefore, the suitable constitutive model of each thickness zone of TRB cannot be described by the traditional unified macroplastic theory model. Nowadays, with the development of finite element technology, the macroscopic formability can be better analyzed by the mesoscopic deformation mechanism of the material through the crystal plastic finite element method (CPFEM)<sup>[8-10]</sup>. Sheikh et al<sup>[11]</sup> studied texture evolution during the simple shear extrusion (SSE) using CPFEM. The results showed that the normal

strains occur and the position of the shear components changes in the pole figure during the SSE without back-pressure, and because of an imperfect reversal strain after a complete pass of the SSE process, the shear components are still dominant. Hu et al<sup>[12]</sup> used CPFEM based on various slip modes to simulate plastic deformation of NiTi. It was found that in the case of large plastic strain of NiTi shape memory alloy under uniaxial compression,  $\{010\}\langle 100\rangle$  slip mode is regarded as unfavorable slip one, which contributes to the formation of  $(001)[0\bar{1}0]$  texture component, while  $\{110\}\langle 100\rangle$  and  $\{110\}\langle 111\rangle$  slip modes facilitate formation of fiber ( $\langle 111\rangle$ ) texture. Han et al<sup>[13]</sup> used CPFEM to predict the crack formation pattern between the two crystal orientations, and the cracks are found to initiate along the direction of slip lines. At present, crystal plasticity theory has been successfully applied to the forming analysis of sheet metal to study the intrinsic reason of macroscopic plastic deformation from microscopic view<sup>[14,15]</sup>.

In this study, crystal plasticity constitutive model of each

Received date: August 29, 2020

Foundation item: National Natural Science Foundation of China (51575406)

Corresponding author: Fu Xiujuan, Ph. D., Professor, School of Materials Science and Engineering, Wuhan Institute of Technology, Wuhan 430073, P. R. China, Tel: 0086-27-87195661, E-mail: fuxiujuan2008@163.com

Copyright © 2021, Northwest Institute for Nonferrous Metal Research. Published by Science Press. All rights reserved.

thickness zone was established by CPFEM from the perspective of mesomechanics based on the microstructural test and the influence of initial texture on the plastic deformation behavior of TRB, which provides new ideas for the study of inhomogeneous plastic deformation of tailor rolled blank.

## 1 Crystal Plasticity Finite Element Model

### 1.1 Polycrystalline geometric model

The samples with the size of 6 mm×8 mm were cut along the rolling direction in the thin area with 1 mm in thickness, the thick area with 2 mm in thickness and the transition zone. After grinding and polishing, the samples with bright mirror surface were prepared, and then the EBSD samples without stress layer were prepared by electropolishing. The samples were characterized by FEI Quanta 650F scanning electron microscope. The samples were bombarded on the inclined sample surface by electron beam, and the scattered electrons formed diffraction patterns on the fluorescent screen. The patterns were processed by image processor and input into the computer system, and the collected data were analyzed and processed by HKL Channel 5 software.

The microscopic model of each thickness zone of CR340 TRB was simplified into a two-dimensional polycrystalline model, which was established by the Voronoi diagram method<sup>[16,17]</sup>, with the  $x$ -axis direction being the rolling direction and the  $y$ -axis direction being the transverse direction. In each polycrystalline geometric model of thin zone, transition zone and thick zone, the size was 100  $\mu\text{m}$ ×30  $\mu\text{m}$ , and it contained 30 crystal grains, and the initial grain size was 10  $\mu\text{m}$ . According to the actual texture ratio, two main textures were distributed in each polycrystalline model. Fig. 1a and 1d show the ODF diagram and polycrystalline geometric model

in thin zone, respectively. The main initial texture is  $\{111\} \langle 0\bar{1}1 \rangle$  and  $\{141\} \langle 2\bar{1}2 \rangle$  accounting for 18 and 12 grains, which are represented by grains B1 and B2 with different colors, respectively. The main initial texture in transition zone is  $\{225\} \langle 1\bar{1}0 \rangle$  and  $\{211\} \langle 0\bar{1}1 \rangle$  accounting for 15 and 15 grains in Fig. 1b and Fig. 1e, which are represented by grains G1 and G2, respectively. The main initial texture in thick zone is  $\{876\} \langle \bar{2}25 \rangle$  and  $\{211\} \langle 0\bar{1}1 \rangle$  accounting for 18 and 12 grains in Fig. 1c and Fig. 1f, which are represented by grains H1 and H2, respectively. In this model, CPS4I (4-node quadrilateral bilinear plane stress non-coordination mode unit) mesh was used to improve the calculation accuracy. There were 3131 nodes and 3000 quadrilateral elements. In addition, the loading strain rate was 0.02  $\text{s}^{-1}$  and the deformation quantity was 20%.

### 1.2 Constitutive model

In the crystal uniform slip model<sup>[18]</sup>, the total deformation gradient  $\mathbf{F}$  can be decomposed as follows:

$$\mathbf{F} = \frac{\partial x}{\partial X} = \mathbf{F}^* \mathbf{F}^P \quad (1)$$

where  $x$  is the position coordinate of the particle in the current configuration,  $X$  is the position coordinate of the particle in the initial configuration,  $\mathbf{F}^*$  is the elastic deformation gradient, and  $\mathbf{F}^P$  is the plastic deformation gradient.

Since the stress during the deformation process is determined only by  $\mathbf{F}^*$ , the relationship between the shear strain caused by the slip in each slip system and the overall plastic deformation gradient can be expressed as follows:

$$\mathbf{F}^P \cdot \mathbf{F}^{P^{-1}} = \sum_{\alpha=1}^N \dot{\gamma}^{\alpha} \mathbf{s}_0^{\alpha} \otimes \mathbf{n}_0^{\alpha} \quad (2)$$

where  $N$  is the number of active slip systems,  $\dot{\gamma}^{\alpha}$ ,  $\mathbf{s}_0^{\alpha}$ ,  $\mathbf{n}_0^{\alpha}$  and  $\mathbf{s}_0^{\alpha} \otimes \mathbf{n}_0^{\alpha}$  are the plastic shear strain rate, the unit vector of the slip direction, the unit normal vector of the slip plane and the

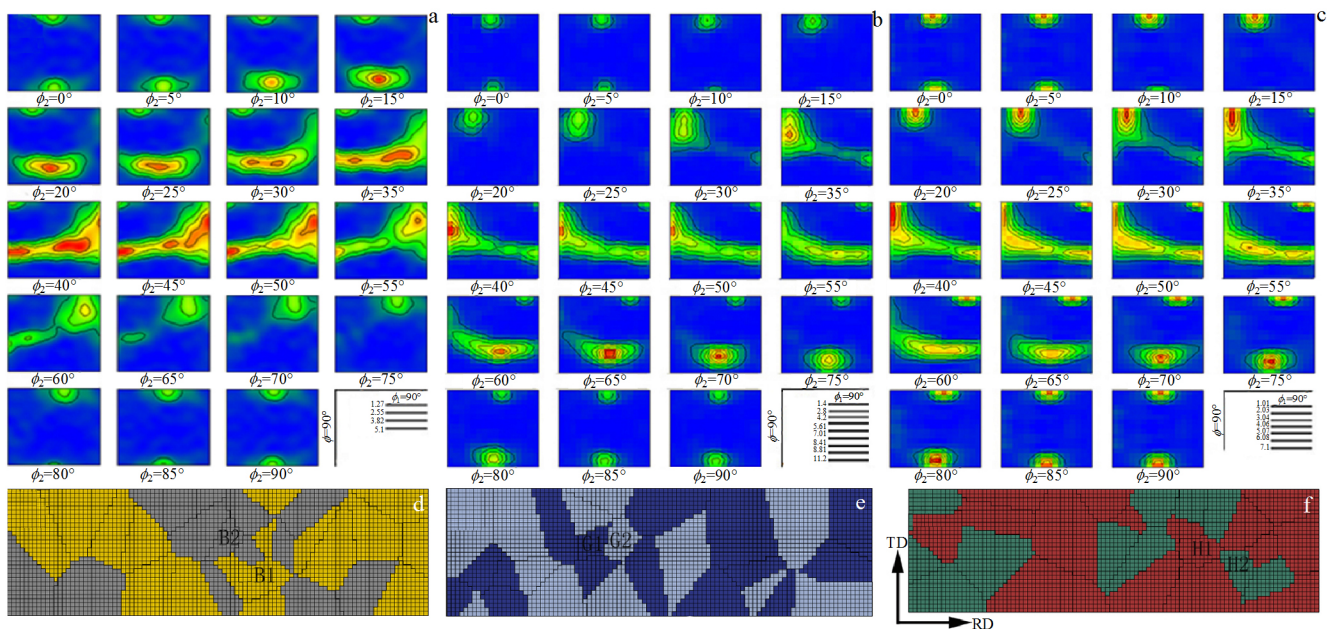


Fig. 1 ODF (a~c) and finite element models (d~f) of different thickness zones: (a, d) thin zone, (b, e) transition zone, and (c, f) thick zone

Schmid tensor of slip system in the reference coordinate system, respectively.

Assuming that slip has no effect on the elastic properties of the crystal, the elastic constitutive equation<sup>[19]</sup> can be prescribed through Eq.(3):

$$\boldsymbol{\tau}^* = \mathbf{C}^* : \mathbf{D}^* \quad (3)$$

where  $\mathbf{C}^*$  is the instantaneous elastic tensor which is a fourth-order tensor,  $\mathbf{D}^*$  is the elastic deformation rate tensor,  $\boldsymbol{\tau}^*$  is the Jaumann derivative of the Kirchhoff stress tensor  $\boldsymbol{\tau}$  with the intermediate configuration as the reference state.  $\boldsymbol{\tau}^*$  and  $\mathbf{D}^*$  can also be expressed as follows:

$$\boldsymbol{\tau}^* = (\mathbf{F}^*)^{-1} [\det(\mathbf{F}) \boldsymbol{\sigma}] (\mathbf{F}^*)^{-1} \quad (4)$$

$$\mathbf{D}^* = \frac{1}{2} [(\mathbf{F}^*)^T \mathbf{F}^* - \mathbf{I}] \quad (5)$$

where  $\boldsymbol{\sigma}$  is the crystal Cauchy stress and  $\mathbf{I}$  is the second-order unit tensor.

Since all grains in the model are given the same boundary conditions during the simulation, the blanks are uniformly deformed, so the stress formula of the polycrystalline polymer proposed by Taylor is used in this study<sup>[20]</sup>.

$$\bar{\boldsymbol{T}} = \sum_{a=1}^n v^a \mathbf{T}^a \quad (6)$$

where  $\bar{\boldsymbol{T}}$  is the volume average stress,  $n$  is the number of polycrystalline grains,  $v^a$  is the volume fraction of the grain  $a$ , which is related to the probability of occurrence of a certain-texture grain;  $\mathbf{T}^a$  is the Cauchy stress of the grain  $a$ .

In the rate-dependent crystal plasticity model, the slip shear rate is determined by the stress state of the current configuration, so the slip rate and the shear stress can be expressed as the following power rate form<sup>[21]</sup>.

$$\dot{\gamma}^a = \begin{cases} \dot{\gamma}_0 \text{sign}(\boldsymbol{\tau}^a) \left| \frac{\boldsymbol{\tau}^a}{\mathbf{g}^a} \right|^n & \boldsymbol{\tau}^a \geq \mathbf{g}^a \\ 0 & \boldsymbol{\tau}^a < \mathbf{g}^a \end{cases} \quad (7)$$

where  $\dot{\gamma}_0$ ,  $\boldsymbol{\tau}^a$ ,  $\mathbf{g}^a$  and  $n$  is the reference strain rate, the resolved shear stress, the slip system resistance and the strain sensitivity exponent in the slip system  $\alpha$ , respectively; sign is a symbolic function.

As the degree of plastic deformation increases, the metal material will undergo work hardening, and the slip system resistance  $\mathbf{g}^a$  will also increase. At the same time, considering that the plastic-mechanical deformation with dislocation of bcc is more complicated, the shear stress calculation formula in the modified slip resistance model<sup>[22]</sup> is proposed. And the evolution formula of  $\mathbf{g}^a$  is as follows:

$$\mathbf{g}_{c,bcc}^a = \mathbf{g}^a - c^a \mathbf{g}_{ng}^a \quad (8)$$

$$\dot{\mathbf{g}}^a = \sum_{\beta=1}^n h_{a\beta} |\dot{\gamma}^\beta| \quad (9)$$

where  $c^a$  is the net effect coefficient of non-slip stress on the effective slip resistance,  $\mathbf{g}_{ng}^a$  is the shear stress on the non-slip plane,  $\mathbf{g}_{c,bcc}^a$  is the corrected slip system resistance, and  $h_{a\beta}$  is the slip hardening modulus, which is a function of the cumulative shear strains on all slip systems.  $h_{a\beta}$  is represented by the following equation<sup>[23,24]</sup>:

$$h_{aa} = h_0 \sec h^2 \left| \frac{h_0 \gamma}{\tau_s - \tau_0} \right| \quad (10)$$

$$h_{a\beta} = q h_{aa} \quad (\alpha \neq \beta) \quad (11)$$

where  $\delta_{\alpha\beta}$  is the Kronecker matrix,  $h_0$  is the initial hardening modulus,  $\tau_s$  is the saturation stress,  $\tau_0$  is the initial value of current strength, and  $q$  is the hardening ratio. When  $\alpha = \beta$ ,  $h_{a\beta}$  is the self-hardening modulus,  $\delta_{\alpha\beta} = 1$ ; then  $\alpha \neq \beta$ ,  $h_{a\beta}$  is the latent hardening modulus,  $\delta_{\alpha\beta} = 0$ . For the high strength low carbon steels, the latent hardening between the slip systems is small, so the value of  $q$  is 1.

### 1.3 Material parameters

In addition to the initial orientation of TRB obtained by EBSD, the material parameters such as elastic modulus and hardening parameters can be determined by the comparative analysis of stress-strain curves obtained by uniaxial tension finite element simulation and experiment. Firstly, the samples were prepared by wire cutting (the size of the test sample is specified according to GB/T228-2010 standard), and then the stress-strain curve was obtained by tensile test at 2 mm/min on AG-100 kN universal testing machine. Through repeated simulation verification, the accurate comparison result was obtained, as shown in Fig. 2. The elastic modulus is characterized by three parameters  $C_{11}$ ,  $C_{12}$  and  $C_{44}$ , and the corresponding material parameters are shown in Table 1. There is no necking section in the stress-strain curve obtained by uniaxial tension finite element simulation because the material fracture is not considered in the simulation calculation.

## 2 Results and Discussion

### 2.1 Effect of initial texture on slip system

The bcc crystal including ferrite crystals has a maximum of 48 slip systems<sup>[23]</sup>. There are 24 sets of slip systems that can only be activated at high temperatures, whose slip plane is

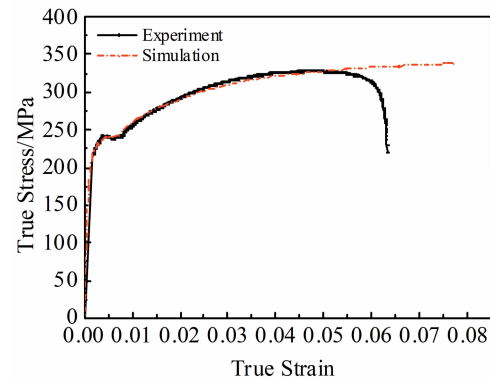


Fig.2 Experimental and simulated stress-strain curves

Table 1 Material parameters of samples

$C_{11}$ /GPa	$C_{12}$ /GPa	$C_{44}$ /GPa	$\dot{\gamma}_0/s^{-1}$	$h_0$ /MPa	$\tau_s$ /MPa	$\tau_0$ /MPa	$q$
230	130	117	0.001	240	68	60	1

{123} and slip direction is  $\langle 111 \rangle$ . While there are 12 sets of slip systems that can only be activated at low temperatures, whose slip plane is {112} and slip direction is  $\langle 111 \rangle$ . Therefore in this study, only the activation of 12 sets of slip systems was studied, whose slip plane is {110} and slip direction is  $\langle 111 \rangle$ . As shown in Table 2, the slip system corresponds to the state variables from SDV49 to SDV60 in the simulation results.

Fig.3 shows shear strain-time curves for six grains (B1, B2, G1, G2, H1, and H2) in different slip systems. The three crystallographic axis of [100]-[010]-[001] corresponds to the coordinate system rolling direction (RD)-transverse direction (TD)-normal direction (ND) of the model, so when the activation direction of the slip is along the opposite direction of the slip system, the shear strain is a negative value. In Fig.3, it can be seen that the slip systems of each grain are not all activated, and the activation sets of slip systems and strain value of each grain are different. As can be seen from Fig.3a, the shear-strain values of the slip systems (101)  $[\bar{1}\bar{1}1]$ , (101)

$[\bar{1}\bar{1}\bar{1}]$ , and (10 $\bar{1}$ )  $[\bar{1}\bar{1}1]$  corresponding to the state variables SDV51, SDV52, and SDV58 are all 0 in the grain B1, which indicates that the three sets of slip systems are not activated. In the 9 sets of activated slip systems, the shear strain of the slip system corresponding to SDV60 has the largest absolute value, which reaches 0.034, indicating that the slip system has the largest degree of actuation on grain B1. And the shear-strain absolute value of the slip system corresponding to SDV54 is only 0.003. In Fig.3b, only 5 sets of slip systems are activated on grain B2, which corresponds to the state variables SDV49, SDV57, SDV58, SDV59 and SDV60. As shown in Fig.3c-3f, 6 sets of slip systems are activated on grain G1, 7 sets of slip systems are activated on grain G2, 8 sets of slip systems are activated on grain H1, and only 6 sets of slip systems are activated on grain H2. The above results show that the activation of the slip system is different due to different orientations of the grains in different thickness zones, where {111} $\langle 0\bar{1}1 \rangle$  and {876} $\langle \bar{2}\bar{2}5 \rangle$  textures are favorable to activate slip systems.

Fig. 4 shows the number of activated grains in the slip system. It can be seen that a total of 223 grains in the thin zone, 215 grains in thick zone, and only 197 grains in transition zone are activated, which indicates that because lots of {111} $\langle 0\bar{1}1 \rangle$  and {876} $\langle \bar{2}\bar{2}5 \rangle$  textures are advantageous for stamping in the equal thickness zones, the sliding systems of more grains are activated. Studies have shown that the more the slip systems are activated, the better the plasticity of the metal, so it can be seen that the plasticity of the equal thickness zones is better than that of the transition zone.

**2.2 Stress and strain distribution**

Generally, the orientation angle with large difference between different textures can make the slip easily blocked at

**Table 2 State variables and corresponding slip system**

Slip system			Slip system		
Slip plane	Slip direction	State variable	Slip plane	Slip direction	State variable
(011)	$[\bar{1}\bar{1}1]$	SDV49	$(0\bar{1}\bar{1})$	[111]	SDV55
	$[\bar{1}\bar{1}\bar{1}]$	SDV50		$[\bar{1}\bar{1}\bar{1}]$	SDV56
(101)	$[\bar{1}\bar{1}1]$	SDV51	$(10\bar{1})$	[111]	SDV57
	$[\bar{1}\bar{1}\bar{1}]$	SDV52		$[\bar{1}\bar{1}\bar{1}]$	SDV58
(110)	$[\bar{1}\bar{1}1]$	SDV53	$(\bar{1}10)$	[111]	SDV59
	$[\bar{1}\bar{1}\bar{1}]$	SDV54		$[\bar{1}\bar{1}\bar{1}]$	SDV60

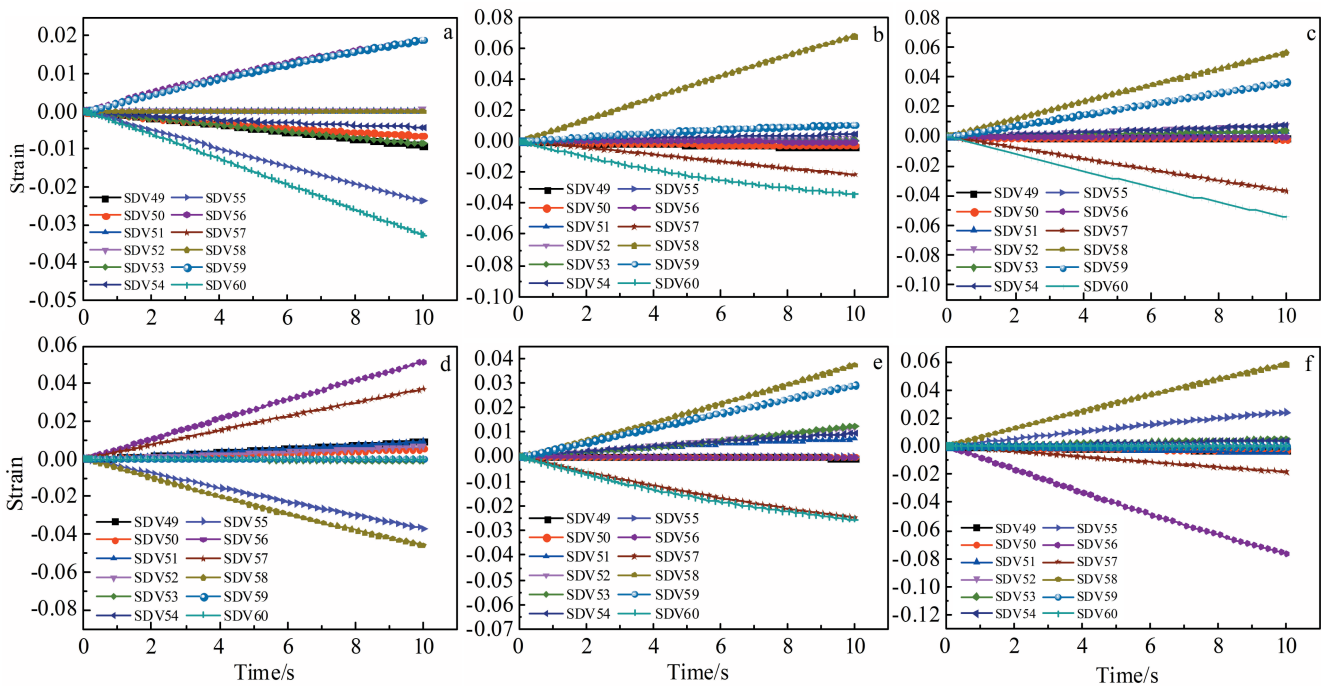


Fig.3 Shear strain-time curves of slip system for different grains: (a) B1, (b) B2, (c) G1, (d) G2, (e) H1, and (f) H2

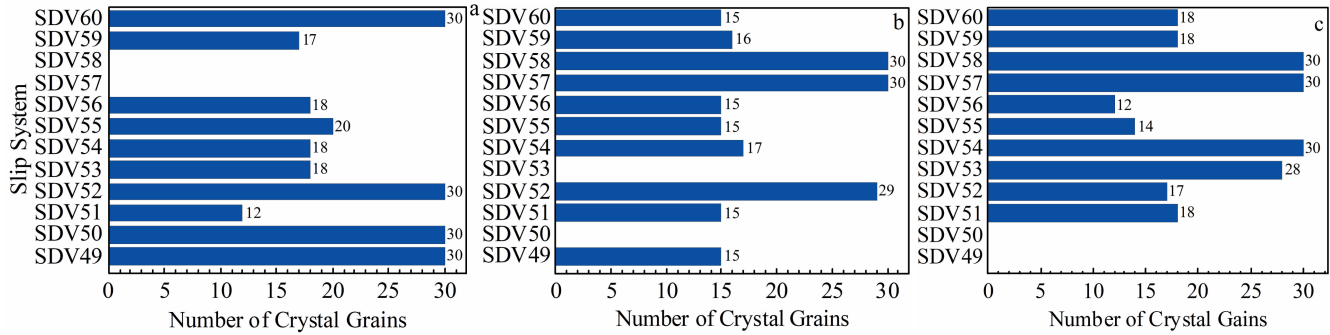


Fig.4 Grain activation number of each slip system for different thickness zones: (a) 1 mm thin zone, (b) the transition zone, and (c) 2 mm thick zone

the grain boundary, resulting in accumulation of dislocations on the grain boundaries and more severe stress concentration, while there is a small difference in the orientation angle between grains with the same texture, and the degree of stress concentration at the grain boundary is also small. In Fig. 5a and 5c, the stress change gradient in equal thickness zones of TRB is large after the deformation, and the stress changes significantly at the grain boundary between grains with different textures, and there is also stress concentration at the grain boundaries between grains with the same texture, where the internal stress concentration is mostly distributed in grains with  $\{141\} \langle 2\bar{1}2 \rangle$  texture in thin zone and  $\{411\} \langle 0\bar{1}1 \rangle$  texture in thick zone. While the grains with  $\{111\} \langle 0\bar{1}1 \rangle$  and  $\{876\} \langle 2\bar{2}5 \rangle$  textures are in the soft orientation, which promotes the activation of the slip and relieves the stress concentration at the grain boundary, causing slip of dislocation at the adjacent grain boundaries and more grains to get the chance of deformation, so that the plasticity of blank increases. It can be clearly seen from Fig. 5b that the entire transition zone is in the stress concentration zone. It is known from the slip system that two textures in the transition zone is not conducive to slip. When the blank is subjected to an external force, grains are difficult to plastically deform. The above results indicate that the plastic deformation of polycrystalline metal materials is closely related to the orientation of grains. The more the grains in the soft orientation, the easier the grains to slip. At this time, the stress concentration is weakened, the brittleness of the material is reduced, and the toughness is improved.

Fig. 6 shows logarithmic strain distribution in different thickness zones of TRB after tension, which has similar characteristics to the stress distribution. As shown in Fig. 6a and Fig. 6c, the strain distribution of the thin and thick regions of the thick plate is inhomogeneous after uniaxial tension. The strain is obviously distributed at the grain boundaries between different textures and a relatively clear strain zone appears in the interior of some grains, so a deformation zone is formed which runs through the entire transverse direction. It is found that the deformation degree of grains with different textures is very different, and there are almost no deformation on grains with  $\{141\} \langle 2\bar{1}2 \rangle$  and  $\{411\} \langle 0\bar{1}1 \rangle$  textures. This is because different textures result in different orders of activation of the

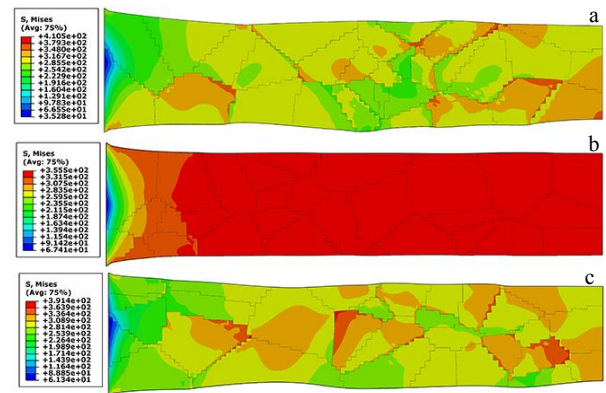


Fig.5 Stress distribution of different thickness zones: (a) thin zone, (b) transition zone, and (c) thick zone

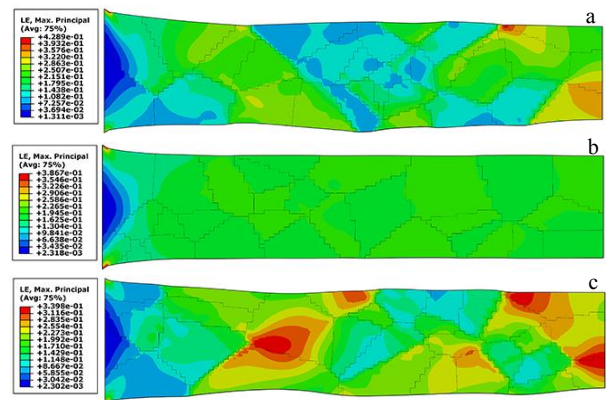


Fig.6 Logarithmic strain distribution of different thickness zones: (a) thin zone, (b) transition zone, and (c) thick zone

slip system, so the strain of grains is inconsistent. At the same time, the deformation of grains is affected by adjacent grains, which also leads to uneven strain distribution of the polycrystalline material. However, the orientation difference between grains in the transition zone is not large, which is not conducive to slip, so there is no obvious strain concentration zone in Fig. 6b.

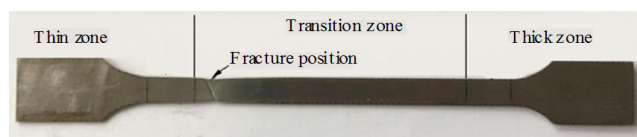


Fig.7 TRB specimen for uniaxial tension experiment

It can be seen from the above analysis and results that there is a favorable crystal orientation in the equal thickness zones of TRB, so the slip systems are easy to be activated and local stress concentration is formed at the grain boundary during plastic deformation, which is beneficial to improve the plastic deformation ability of the material. But the textures in the transition zone is not conducive to slip, so when subjected to an external force, the grains are hard to be plastically deformed, thereby causing stress concentration throughout the transition zone. Therefore, the inhomogeneous initial texture in the transition zone leads to poor plastic deformation ability and stress concentration, resulting in excessive thinning or cracking. The results also accurately predict that the fracture position of TRB in uniaxial tension experiment will appear in the transition zone. And the result of uniaxial tension experiment of TRB is shown in Fig.7.

### 3 Conclusions

1) In the case of tensile plastic deformation, the  $\{111\} \langle 0\bar{1}1 \rangle$  texture of the thin zone and the  $\{876\} \langle \bar{2}25 \rangle$  texture of the thick zone are conducive to the activation of the slip system, and their plastic deformation capacity is higher than that of the transition zone; in the grains of these two textures, the activation number of the slip system is 9 and 8 sets, and the total number of grain slip systems in the thin and thick zones is 223 and 215, respectively. However, in the transition zone, only 6 and 7 sets of slip systems are activated in the grains of the  $\{225\} \langle 1\bar{1}0 \rangle$  and  $\{211\} \langle 0\bar{1}1 \rangle$  textures, and the total number of grain slip systems activated is 197.

2)  $\{111\} \langle 0\bar{1}1 \rangle$  and  $\{876\} \langle \bar{2}25 \rangle$  textures are in a soft direction, which is conducive to relieving the stress concentration generated between grains, and grains are easier to slip, so the brittleness of the thin and thick zones is reduced, and plastic deformation is prone. However, the inhomogeneity of the initial texture for the grains in the transition zone makes the post-tensile stress high and widely distributed, and the plastic deformation ability is poor, so it can accurately predict the fracture location in the transition zone.

### References

- 1 Shafiei E, Dehghani K. *Vacuum*[J], 2017, 143: 71
- 2 Sun G Y, Tian J, Liu T Y et al. *Engineering Structures*[J], 2018, 169: 201
- 3 Ke D W, Liu X H, Zhi Y et al. *Materials Science & Engineering A*[J], 2019, 742: 629
- 4 Kim D, Kim J, Lee Y et al. *Rare Metals*[J], 2006, 25(6): 111
- 5 Krux R, Homberg W, Kleiner M. *Steel Research*[J], 2005, 76(12): 890
- 6 Meyer A, Wietbrock B, Hirt G. *International Journal of Machine Tools & Manufacture*[J], 2008, 48(5): 522
- 7 Zhang H W, Liu L Z, Hu P et al. *Journal of Iron and Steel Research International*[J], 2012, 19(9): 8
- 8 Li L T, Lin Y C, Li L et al. *Journal of Materials Engineering & Performance*[J], 2015, 24(3): 1294
- 9 Kim D K, Kim J M, Park W W et al. *Computational Materials Science*[J], 2015, 100: 52
- 10 Kim J H, Lee M G, Kang J H et al. *International Journal of Plasticity*[J], 2017, 93: 26
- 11 Sheikh H, Ebrahimi R, Bagherpour E. *Materials & Design*[J], 2016, 109: 289
- 12 Hu L, Jiang S Y, Zhang Y Q et al. *Progress in Natural Science*[J], 2017, 27(5): 598
- 13 Han Q N, Qiu W H, He Z W et al. *Tribology International*[J], 2018, 125: 209
- 14 Zhang K, Holmedal B, Hopperstad O S et al. *International Journal of Plasticity*[J], 2015, 66: 3
- 15 Xu Z T, Peng L F, Fu M W et al. *International Journal of Plasticity* [J], 2015, 68: 34
- 16 Merland R, Caumon G, Lévy B et al. *Computational Geosciences* [J], 2014, 18: 373
- 17 Ghosh S, Lee K, Moorthy S et al. *International Journal of Solids and Structures*[J], 1995, 32(1): 27
- 18 Asaro R J, Rice J R. *Journal of the Mechanics and Physics of Solids*[J], 1977, 25(5): 309
- 19 Hill R, Rice J R. *Journal of the Mechanics and Physics of Solids* [J], 1972, 20(6): 401
- 20 Taylor G I. *Journal of the Institute of Metals*[J], 1938, 62: 307
- 21 Hutchinson J W. *Proceedings of the Royal Society of London*[J], 1976, 348(1652): 101
- 22 Vitek V, Mrovec M, Gröger R et al. *Materials Science and Engineering*[J], 2004, 387-389: 138
- 23 Asaro R J, Needleman A. *Acta Metallurgica*[J], 1985, 33(6): 923
- 24 Peirce D, Asaro R J, Needleman A. *Acta Metallurgica*[J], 1983, 31(12): 1951

## 初始织构对差厚板非均匀塑性变形的影响

付秀娟, 鲁江, 赵严, 叶港

(武汉工程大学材料科学与工程学院, 湖北 武汉 430073)

**摘要:** CR340 轧制差厚板 (TRB) 在轧制过程中, 其不同的厚度区形成了不同的织构, 分别是薄区的  $\{111\}\langle 0\bar{1}1\rangle$  和  $\{141\}\langle 2\bar{1}2\rangle$  织构, 过渡区的  $\{225\}\langle 1\bar{1}0\rangle$  和  $\{211\}\langle 0\bar{1}1\rangle$  织构, 厚区的  $\{876\}\langle 2\bar{2}5\rangle$  和  $\{411\}\langle 0\bar{1}1\rangle$  织构。根据 EBSD 测试结果, 建立了各厚度区的多晶体塑性有限元模型, 研究了单向拉伸时各厚度区的晶粒织构对滑移系开动情况和应力应变分布的影响规律。结果表明, 薄区的  $\{111\}\langle 0\bar{1}1\rangle$  织构和厚区的  $\{876\}\langle 2\bar{2}5\rangle$  织构有利于滑移系的开动, 开动的数量分别为 9 和 8 组, 这使得等厚区在变形中的应力集中弱化, 具有良好的塑性变形行为。而过渡区的  $\{225\}\langle 1\bar{1}0\rangle$ 、 $\{211\}\langle 0\bar{1}1\rangle$  织构的晶粒滑移系开动较少, 开动的数量分别为 6 和 7 组, 导致应力集中, 其塑性变形行为较差。差厚板各厚度区织构的差异导致其塑性变形呈现明显的不均匀性, 其断裂位置发生在单轴拉伸时塑性变形较差的过渡区。

**关键词:** 差厚板; 晶体塑性有限元法; 织构; 塑性变形; 滑移系

**作者简介:** 付秀娟, 女, 1974 年生, 博士, 教授, 武汉工程大学材料科学与工程学院, 湖北 武汉 430073, 电话: 027-87195661, E-mail: fuxiujuan2008@163.com